Accepted Manuscript

Title: Fast and simple assessment of surface contamination in operations involving nanomaterials

Authors: Alberto Clemente, Raquel Jiménez, M. Mar Encabo, M. Pilar Lobera, Francisco Balas, Jesus Santamaria

PII: S0304-3894(18)30902-6
DOI: https://doi.org/10.1016/j.jhazmat.2018.10.011
Reference: HAZMAT 19831

To appear in: *Journal of Hazardous Materials*

Received date: 10-7-2018
Revised date: 1-10-2018
Accepted date: 3-10-2018

Please cite this article as: Clemente A, Jiménez R, Mar Encabo M, Lobera MP, Balas F, Santamaria J, Fast and simple assessment of surface contamination in operations involving nanomaterials, *Journal of Hazardous Materials* (2018), https://doi.org/10.1016/j.jhazmat.2018.10.011

This is a PDF file of an unedited manuscript that has been accepted for publication. As a service to our customers we are providing this early version of the manuscript. The manuscript will undergo copyediting, typesetting, and review of the resulting proof before it is published in its final form. Please note that during the production process errors may be discovered which could affect the content, and all legal disclaimers that apply to the journal pertain.

ACCEPTED MANUSCRIPT

Fast and simple assessment of surface contamination in operations involving nanomaterials

Alberto Clemente,[†] Raquel Jiménez,[†] M. Mar Encabo,[†] M. Pilar Lobera,[†‡] Francisco Balas,[†‡*] & Jesus Santamaria[†‡*]

[†]Instituto de Nanociencia de Aragón (INA) – Universidad de Zaragoza, c/ Mariano Esquillor s/n, 50018 Zaragoza (Spain).

[‡]Networking Biomedical Research Centre for Biomaterials, Bioengineering and Nanomedicine (CIBER-BBN), c/ Monforte de Lemos 28, 28040 Madrid (Spain).

[*]Corresponding authors.

Highlights

- Surface contamination caused by handling nanomaterials was traced using fluorescently labeled 80-nm silica nanoparticles.
- Fluorescent silica nanoparticles granted high analytical sensibility, small sizes and high dispersability in aerosol phase.
- Below 100 ppm of fluorescent nanoparticles added to the aerosol matter allowed exposure assessment in wide contact surfaces.
- The appropriate illumination revealed the deposition zones, allowing a low-cost procedure for risk assessment tests.

Abstract

ACCEPTED MANUSCRIPT

The deposition of airborne nanosized matter onto surfaces could pose a potential risk in occupational and environmental scenarios. The incorporation of fluorescent labels, namely fluorescein isotiocyanate (FITC) or tris-1,3-phenanthroline ruthenium (II) chloride ($Ru(phen)_3Cl_2$), into spherical 80-nm silica nanoparticles allowed the detection after the illumination with LED light of suitable wavelength (365 or 405 nm respectively). Monodisperse nanoparticle aerosols from fluorescently labeled nanoparticles were produced under safe conditions using powder generators and the deposition was tested into different surfaces and filtering media. The contamination of gloves and work surfaces that was demonstrated by sampling and SEM analysis becomes immediately clear under laser or LED illumination. Furthermore, nanoparticle aerosols of about 10^5 nanoparticles/cm^3 were alternatively fed through a glass pipe and personal protective masks to identify the presence of trapped nanoparticles at under 405 nm or 365 nm LED light. This testing procedure allowed a fast and reliable estimation of the contamination of surfaces with nanosized matter, with a limit of detection based on the fluorescence emission of the accumulated solid nanoparticles of 40 ng of $Ru(phen)_3@SiO_2$ of silica per mg of non-fluorescent matter.

Introduction

Thanks to the unique properties of nanomaterials, the global nanotechnology market is expected to grow at a compound annual growth rate of around 17% during the period 2017-2024 [1], giving rise to a variety of nanotechnology-enabled products. These same new properties may give rise to new risks and uncertainties and the scientific community has been aware of the possibility of nanomaterials having an adverse impact on human health or the environment for more than two decades [2-8]. The main concern, however, has always been the inhalation of nanoparticles [9-11] and indeed measuring nanoparticle aerosol concentration is part of the standard procedure in any assessment of exposure to nanoparticles in the workplace and the environment [10-13]. Fortunately, a number of commercial instruments have become available to measure number and size distribution in nanoparticle aerosols, solving one of the challenges identified by Maynard *et al.* [14] in the development of sustainable

ACCEPTED MANUSCRIPT

nanotechnologies. Also, current engineering controls and personal protective equipment have been shown to be highly effective at providing worker protection during the handling of nanomaterials [15,16].

However, there are other aspects that are often overlooked when considering possible exposure scenarios. Among these, the inadvertent contamination of surfaces that could have been exposed to nanoparticles stands out as the main concern, on account of two main reasons. The first aspect relates to the contact of unprotected skin with surfaces that are contaminated with nanoparticles. It is generally accepted that one should not use presumably contaminated gloves when touching surfaces in common areas: the *one-glove policy* (see for instance [17]) and similar approaches imply that bare hands should be used to touch common-area surfaces such as handles, computer and instrument keyboards, electrical switches and so on. If these surfaces were contaminated with nanoparticles, anyone touching them unprotected would be subjected to skin contact with nanoparticles with subsequent risks associated to different entry routes: dermal, ingestion, etc. It is thus necessary to have some means of detection of nanoparticle contamination on common-area surfaces that can be touched unprotected. However, detection of nanomaterials contamination on surfaces is usually a laborious procedure. In previous works [18,19], we used rare earth labeling of TiO_2 nanoparticles to monitor surface contamination during handling operations followed by sampling and TEM-EDX analysis or elemental analysis (ICP-OES) of digested wipes after cleaning the suspect area. Similarly, Hedmer *et al*. [20] used adhesive tape sampling followed by electron microscopy to detect contamination by carbon nanotubes and nanodiscs of work surfaces at a small-scale manufacturer. All of these works involve complex procedures requiring expensive instruments and specialized personnel.

In addition to skin contact, the second aspect of concern is that nanoparticle-contaminated surfaces themselves may become points of generation of secondary aerosols that could be subsequently inhaled. The opportunities are ample and include handling of polluted laboratory items (lab coats, masks, instruments), operation on surfaces close to handling areas outside fume hoods (laboratory

ACCEPTED MANUSCRIPT

benches close to weighting stations are a common example), and cleaning of laboratory surfaces and instruments, which is often carried out by external (usually non-scientific) personnel. Studies related to the generation of aerosols from work surfaces and clothing contaminated by nanomaterial handling are extremely rare. Ding *et al.* [21] recently reviewed worker exposure during different handling activities. They pointed out that some low-energy activities, including cleaning, could result in the release of airborne nanoparticles. Tsai [22] investigated the release of nanomaterials associated to the handling of clothing contaminated with nanoparticles and found that the release of airborne nanoparticles depended on the type of fabric, with cotton showing the highest release levels. Schneider *et al.* [23] discussed the dustiness and degree of agglomeration of nanomaterials in relation to personal exposure, and also recognized the role of contaminated surfaces as potential sources of secondary aerosols. All of these studies provide valuable insight on the phenomena involved in respirable aerosol generation from contaminated sources and on the complexity of the evaluation of the risks involved, but do not provide a simple method to spot this contamination.

Here we present a simple procedure to detect surface contamination caused by operations involving the handling of nanomaterials. We have adapted a synthesis procedure to obtain un-aggregated, fluorescently labeled silica nanoparticles with a particle size around 80 nm. These nanoparticles present several important advantages as markers of surface contamination: (i) the fluorescent molecules are trapped in the core of the particle, *i.e.* the surface consists essentially of unmodified silica; (ii) the particles are highly fluorescent and this allows detection even at very low concentration in the presence of a strong dilution by non-fluorescent background material; (iii) their small size and un-aggregated nature means that they will be dispersed easily in handling operations and travel longer distances. This is a well-known technique to visualize and quantify the nanosized matter in cell studies and biological media [24]. Because of these characteristics, they constitute excellent candidates as added-on tags to other nanomaterials in risk assessment of operations involving the handling of nanomaterials. Thus, to evaluate the extent of contamination caused by a specific handling

ACCEPTED MANUSCRIPT

operation (*e.g.* weighting, cleaning laboratory synthesis equipment, bagging of nanosized materials) a small proportion of fluorescent nanoparticles would be added to the material being handled. Subsequently, a simple inspection under laser or LED light illumination would reveal the area likely affected by the contamination. The results obtained are surprisingly sensitive and provide an easy, low-cost procedure to identify likely contaminated areas during risk assessment exercises.

Experimental section

Synthesis and characterization of labeled nanoparticles

Two different fluorescent silica nanoparticles were used in this study; green FITC@SiO_2 and reddish Ru(phen)$_3$@SiO_2. The FITC@SiO_2 nanoparticles were synthesized by a water-in-oil emulsion procedure at 20ºC using fluorescein isothiocyanate (FITC, 99 %; Sigma-Aldrich) from cyclohexane (98 %, Sigma-Aldrich), deionized water, Triton X-100 (99 %; Sigma-Aldrich) as surfactant and tetraethyl orthosilicate (TEOS, 98 %; Sigma-Aldrich) as silica precursor [25]. The fluorescent labels were obtained by reacting under Ar atmosphere a mixture of FITC and 3-aminopropyl triethoxysilane (APTES, 99 %; Sigma-Aldrich). This FITC-APTES conjugate was then added to the microemulsion system in presence of monosodium 3-(trihydroxysilyl)propyl methyl phosphonate (THPMP, 50 wt. % in H_2O; Sigma-Aldrich) to promote the electrostatic repulsion of FITC-APTES groups attached to the SiO_2 surface during nanoparticle growth. Red fluorescent Ru(phen)$_3$@SiO_2 nanoparticles were prepared using the Stöber method in ethanol media [26]. TEOS was used as silica source and tris-(1,10-phenanthroline)-ruthenium (II) chloride monohydrate ($Ru(phen)_3Cl_2 \cdot H_2O$, 98%; Sigma-Aldrich) acted as fluorescent label. The synthetic procedure was carried out in the dark under alkaline conditions using ammonium hydroxide (NH_4OH, wt. 28 % in H_2O, Sigma-Aldrich).

The synthesized fluorescent SiO_2 nanoparticles were characterized by electron microscopy. Transmission electron microscopy (TEM) images were taken using a Tecnai T20 (FEI Co., Hillsboro, OR) electron microscope at 200 kV. The particle size distribution corresponding to TEM images was statistically estimated using ImageJ processing software with a number of measured particles over 75 in

ACCEPTED MANUSCRIPT

every image (N > 75). Scanning electron microscopy (SEM) images were obtained using a FEI Inspect field emission gun electron microscope. The particle size distributions in the colloidal state were calculated using dynamic light scattering (DLS) were in a Brookhaven 90Plus instrument. With this technique, the hydrodynamic diameter and ζ-potential of the SiO_2 suspensions in water were estimated.

Analysis of the deposition of nanoparticle aerosols

For testing the aerosol deposition on selected surfaces in the exposure environment, two different procedures were chosen. Firstly, the aerosol emission during nanoparticle handling was tested into a specially designed glove-box chamber of 0.27 m^3. The experiment entailed the transfer inside the chamber of 500 mg of fluorescently labeled SiO_2 dry powdered nanoparticles between two plastic beakers in ten consecutive pouring additions. During the testing, the filled beaker was held with the left hand while the spatula was used to displace the solid using the right hand. Before the experiment, the background aerosol particles inside the chamber were removed by flowing dry and HEPA-filtered air into the chamber for 1 h before the tests. During the experiment the inner atmosphere was kept still for avoiding parasite air currents that could affect the aerosol formation. Finally, the test was repeated three times for ensuring the adequate repeatability of the formed aerosol clouds within the test environment.

Alternatively, stable nanoparticle aerosol streams were produced for testing the deposition in filter facemasks and gas conduction networks. To this end, two different aerosol generators were used for the production of nanoparticulate aerosols of fluorescent SiO_2 nanoparticles. For the $Ru(phen)_3@SiO_2$ nanoparticles, aerosols were produced using the fluidized bed aerosol generator (FBAG) technique as described elsewhere [27]. For the FITC@SiO_2 nanoparticles, a pressure pulse nanoparticle aerosol generator was operated as previously reported [28]. Stable aerosols were obtained from dried powders of the fluorescently labeled nanoparticles, for long periods and with a negligible agglomeration effect. The total particle concentration of the FITC@SiO_2 nanoparticles reached a value about $5 \cdot 10^5$ p/cm^3 at the beginning of the generation experiment (Figure S2) and decayed progressively to about $4 \cdot 10^5$ p/cm^3 after 90 min. The particle size distribution was estimated in three consecutive

ACCEPTED MANUSCRIPT

experiments about 30 min after the starting of the generation tests, showing the emission of nanoparticles in the related size range (CMD 67 ± 7 nm). In the case of the aerosol generated with $Ru(phen)_3@SiO_2$ the concentration of nanoparticles reached a total value of about $1.5 \cdot 10^5$ p/cm^3 (Figure S2). The particle size distribution was estimated in three consecutive scans about 30 min after starting the generation tests, showing the emission of nanoparticles in the related size range (CMD 100 ± 10 nm).

The deposition of the fluorescent nanoparticle in personal protective equipment was tested using a special mannequin system wearing a 3M Aura 9332+ FFP3 (NIOSH N95) facemask located inside the glove-box chamber (Figure S3). Breathing through the filter media was simulated using a pump at 30 l/min and the aerosol concentration in the exposure chamber was set around 10^5 #/cm^3 using the above-mentioned aerosol generators for both $FITC@SiO_2$ and $Ru(phen)_3@SiO_2$ nanoparticles. As expected, the conventional FFP3 filters were very effective to retain nanoparticles when fitting guidelines were followed. The theoretical calculations of the filtration efficiency of facemasks suggested that less than 1% of the particles about 1 μm are collected in the initial layer, whereas the most penetrating particle size fell down to 200 nm for the internal layers [29]. Finally, the nanoparticle aerosol transport and deposition in conductions was tested in a convoluted glass pipe system with a total pipe length of 50 cm and several 90º bents, restrictions and velocity changes (Figure S4). The inner diameter of the conduction was of 0.72 cm in the wide areas to 0.25 cm in the narrow conductions.

Aerosol characterization

Nanoparticulate aerosols were characterized in the range of 5 to 500 nm, using a NPS 500 aerosol spectrometer (Particle Measuring Systems, Boulder CO). For large particle sizes, from 300 nm to 20 μm, an OPC spectrometer (Grimm-Aerosol, Ainring, Germany) was used. The flow rates of both instruments were 0.2 and 1.2 l/min respectively. Aerodynamic behavior of the nanoparticle aerosols was studied through the analysis of the total particle number concentration (TPC) and particle size

ACCEPTED MANUSCRIPT

distributions (PSD) in both NPS and OPC instruments. The PSD were fitted using a lognormal probability density function whenever possible [30].

The SEM images of the deposited nanoparticles were taken by placing 1-cm^2 adhesive carbon tape sections located at 10 cm away from the emission source during the transferring experiments. Also, similar carbon tape sections were placed on the gloves inside the chamber during the handling tests to simulate the deposition in hands.

Fluorescence characterization

Fluorescent emission of the deposited nanoparticles was ascertained by irradiating the contact surfaces with monochromatic light at the adequate wavelengths. In the case of complex filtrating media, the fluorescence of the collected nanoparticles was determined by means of confocal microscopy (Olympus FV10-I, Tokyo, Japan) in every one of the layers of the barrier tissue. Sample illumination was performed using a laser light at 405 nm for $Ru(phen)_3@SiO_2$ and at 473 nm for $FITC@SiO_2$, the emission wavelengths were measured at 575 and 516 nm respectively. For 3D image reconstruction, the built-in FV10-Asw 2.1 Viewer software was used after 90 successive images in parallel planes separated 2 μm.

Results and discussion

Two different types of fluorescent nanoparticles were prepared for the generation of nanoparticulate aerosols, containing fluorescein isothiocyanate (FITC) (green) or a Ru(II) phenanthroline complex ($Ru(phen)_3Cl_2$) (reddish) as fluorescent labels. These are denoted as $FITC@SiO_2$ and $Ru(phen)_3@SiO_2$ respectively. The synthesis conditions were chosen to give a narrow size distribution of mostly un-aggregated silica particles containing a specific fluorescent compound. Their main characteristics, (fluorescent emission in aqueous suspension, morphology and particle size distribution) are given in Figure 1. In both cases a spherical or near-spherical morphology was obtained, with size distributions centered about 80 nm. Emitted fluorescence from nanoparticle suspensions was narrow, which allowed detection in liquid phase even at low concentrations [31]. Using these

ACCEPTED MANUSCRIPT

nanoparticles, aerosols were generated using a variety of techniques. Unintended nanoparticle emission during a usual laboratory operation was simulated by accidental aerosol generation during the transfer of fluorescent nanoparticles between two beakers. Alternatively, well-defined, steady aerosols streams containing nanoparticles with a known concentration were generated either with a fluidized bed aerosol [27] generator or with a pressure-pulse generator [28]. These nanoparticle-containing streams were then passed through a network of glass pipes or through filtering masks to assess surface deposition. Figure 2 gives the particle size distributions in the generated aerosol streams and a SEM picture of nanoparticles collected in a filter directly from the aerosol. It can be seen that the nanoparticle aerosols are largely non-agglomerated, with their average particle sizes close to those of the primary nanoparticles.

Contamination of work surfaces during handling

The transfer of 500 mg of $Ru(phen)_3@SiO_2$ nanoparticles between two beakers (see experimental section for details and also Figure S1, in supplementary information) inside a glove chamber was repeated 10 times. Some dustiness was apparent after the transfer in the work area (between the gloves), though other areas in the chamber were apparently clean at plain sight. SEM observation of samples taken from the surface of the gloves and on the work surfaces showed the presence of agglomerates with a size of up to tens of microns. On a closer look, it can be seen that these aggregates are made up of individual nanoparticles (Figure 3a-c). However, the contamination of gloves and work surfaces that was demonstrated by sampling and SEM analysis becomes immediately clear under laser or LED illumination at 405 mm (Figure 3d). Brightly highlighted areas reveal the areas of greater accumulation of $Ru(phen)_3@SiO_2$ nanoparticles on the glove surfaces, on the work area and on the floor of the chamber, near the resting place of the gloves. As explained, in these areas contamination is expected and even some dust can be observed on close visual examination. However, this contamination is not apparent on other areas in the glove chamber (e.g. the wall above the glove inserts) that appear to be particle-free on plain sight but are covered by nanoparticles upon LED illumination (Figure 3e). Figure 3f shows a photograph taken from the opposite corner of the chamber, where the surface appears to be

ACCEPTED MANUSCRIPT

completely clean. However, when a 405 nm laser is shone through the transparent methacrylate wall, the presence of nanoparticles becomes immediately clear (Figure 3g). The image is even clearer when taken in the dark (Figure 3g). Therefore, under illumination by a 405 nm LED or laser light, all surfaces in the testing chamber were contaminated after fluorescent nanoparticle handling.

Contamination of surfaces exposed to nanoparticle-containing streams

Given the sensitivity of fluorescent labeling to identify surface contamination, we decided to test the ability of the method to discriminate regions of preferential deposition of nanoparticles on specific locations of generally contaminated surfaces. To this end, we produced a stable nanoparticle aerosol stream with a concentration of *ca.* 10^5 nanoparticles/cm^3 (see Figure S2 supplementary information) and fed it through a convoluted glass pipe system, with pronounced turns and different flow sections (see Figure 4a). To minimize deposition, a high flow rate of 2.0 l/min was used, giving linear velocities from 0.8 to 7 m/s, depending on the local cross sectional area. Figure 4b-f show close-ups of different sections of the glass pipe illuminated with LED light of suitable wavelength (365 or 405 nm) after passing aerosols with FITC@SiO_2 or $Ru(phen)_3$@SiO_2 nanoparticles. While fluorescence corresponding to deposited nanoparticles can be observed at any point on the pipe wall, some areas are clearly subjected to greater deposition intensity, *e.g.* the corners of 90º elbows or the impinging surfaces in T-shaped junctions. Fluorescent labeling provides a simple way to identify areas of higher nanoparticle accumulation.

Nanoparticle-containing aerosol streams were also used to test deposition on facemasks. To this end, a common particulate mask filter was fitted to a mannequin head with a backside exit to draw a continuous air stream. Respiration mask filters with different characteristics [32] are commonly used to protect personnel from particle aerosols in workplaces and several guidelines have been issued for their use and disposal [33]. Nevertheless, the outside of mask filters may become contaminated during use. Also, while most studies of personal protection equipment deal with overall retention efficiency, it would be useful to have a direct measurement of the penetration of nanoparticles in the different layers

ACCEPTED MANUSCRIPT

of the filter mask. The use of FITC@SiO_2 or $Ru(phen)_3$@SiO_2 fluorescent nanoparticles provides a straight forward procedure to assess the penetration of nanosized matter through the filter pieces.

Figure 5 shows the appearance of the mask after being exposed to both types of nanoparticles at plain sight (no apparent contamination) and under 405 nm or 365 nm LED light for masks exposed to a flow of air containing nanoparticles. As can be seen, the presence of nanoparticles on the outer surface of the masks becomes apparent under suitable LED light. Also, when the different layers of the respirator mask were subjected to confocal microscopy examination, it was possible to determine the penetration of the nanoparticles into the mask from the observed luminescence. As expected, it can be seen that the two outermost layers, #1 and #2, constituted by thick fibers (see Figures S3 and S4) contain nanoparticles throughout their thickness (see left panels at the bottom of Figure 5), and similarly, the upstream side of layer 3 is also laden with luminescent nanoparticles. However, the downstream side of layer 3 appears free from luminescence throughout the confocal penetration depth, indicating that nanoparticles have been retained away from the side in contact with the mannequin face.

Finally, the above experiments have demonstrated the ability of fluorescent nanoparticles to act as tags of nanoparticle contamination in a variety of applications. However, in a hypothetical scenario where these particles are used as detectors of potential of surface contamination they would likely be mixed with other nanomaterials being handled, and surface contamination would take place with a mixture of labeled and unlabeled nanoparticles, rather than with fluorescent nanoparticles alone. For this reason, it was deemed necessary to estimate the lowest concentration of fluorescently labeled nanoparticles that would produce sufficient emission to be detected in solid phase. The establishment of such limit of detection (LoD) is a common feature in fluorescent spectrometry in liquid phase using conventional photoluminescence detectors. However, determination of a LoD for fluorescent emission in solid phase is considerably more difficult. We decided to follow a practical approach by blending fluorescent and plain SiO_2 nanoparticles in different amounts to obtain a dilution matrix and to examine the fluorescence of the different proportions. To this end, we deposited a 200-µl drop of an ethanol

ACCEPTED MANUSCRIPT

suspension of a suspension of $Ru(phen)_3@SiO_2$ nanoparticles blended with non-fluorescent SiO_2 nanoparticles at different ratios onto 1-cm glass substrates and allowed to evaporate. The fluorescent emission of the deposited solid particles from the glass substrates was subsequently observed under a 405-nm laser light. In the absence of diluent silica, a concentration of 0.2 mg/l of $Ru(phen)_3@SiO_2$ was enough to produce a detectable signal after evaporation. As the fluorescent nanoparticles were diluted with non-labeled SiO_2 the signal was less strong. In spite of this, the fluorescence of the was strong enough to give low detection limits: Figure 6 shows that a clear signal was still obtained at 40 ng of $Ru(phen)_3@SiO_2$ of silica per mg of non-fluorescent silica, *i.e.* a concentration of 40 ppm.

Conclusions

In summary, labeling with fluorescent labeling provides a powerful tool to detect the presence of nanoparticles on surfaces even at low concentrations. With this simple procedure, we have been able to demonstrate surface contamination in a variety of scenarios (nanoparticle handling, flow of aerosols, use of protective equipment). This is a low cost assessment procedure that could be easily implemented in the analysis of exposure during nanomaterials handling.

Acknowledgments

Funding from the European Union 7th Framework Programme under the project "NanoValid, Development of reference methods for hazard identification, risk assessment and LCA of engineered nanomaterials" (Grant Agreement #263147). F. B. thanks financial support from the Ministry of Economy and Competitiveness of Spain (MINECO) 'Ramón y Cajal' Programme (Contract RYC-2011-07641). M. P. L. thanks financial support from the MINECO 'Juan de la Cierva' Programme (Contract JCI-2012-13421). Finally, financial support from the Government of Aragon and European Social Fund were gratefully acknowledged.

References

ACCEPTED MANUSCRIPT

1. Research and Markets, Inc., Global Nanotechnology Market Outlook 2024. https://www.researchandmarkets.com/reports/3989533/global-nanotechnology-market-outlook-2024 (accessed 5 July 2018).
2. G. Oberdörster, J. Ferin, R. Gelein, S. C. Soderholm, J. Finkelstein, Role of the alveolar macrophage in lung injury: Studies with ultrafine particles, *Environ. Health Persp.* 97 (1992) 193-199.
3. A. Nel, T. Xia, L. Mädler, N. Li, Toxic potential of materials at the nanolevel, *Science* 311 (2006) 622-627.
4. M. A. Dobrovolskaia, S. McNeil, Immunological properties of engineered nanomaterials, *Nat. Nanotechnol.* 2 (2007) 469-478.
5. N. Lewinski, V. Colvin, R. Drezek, Cytotoxicity of nanoparticles, *Small* 4 (2008) 26-49.
6. A. D. Ostrowski, T. Martin, J. Conti, I. Hurt, B. H. Harthorn, Nanotoxicology: characterizing the scientific literature, 2000-2007, *J. Nanopart. Res.* 11 (2009) 251-257.
7. H. F. Krug, P. Wick, Nanotoxicology: An interdisciplinary challenge, *Angew. Chem. Int. Ed.* 50 (2011) 1260-1278.
8. H. F. Krug, Nanosafety research – Are we on the right track? *Angew. Chem. Int. Ed.* 53 (2014) 12304-12319.
9. F. Balas, M. Arruebo, J. Urrutia, J. Santamaria, Reported nanosafety practices in research laboratories worldwide, *Nat. Nanotechnol*. 5 (2010) 93-96.
10. European Agency for Safety and Health at Work, Workplace exposure to nanoparticles (2009). https://osha.europa.eu/es/tools-and-publications/publications/literature_reviews/workplace_exposure_to_nanoparticles (Accessed 5 July 2018)
11. C. Geraci, D. Heidel, C. Sayes, L. Hodson, P. Schulte, A. Eastlake, S. Brenner, Perspectives on the design of safer nanomaterials and manufacturing processes, *J. Nanopart. Res*. 17 (2015) 366-379.

ACCEPTED MANUSCRIPT

12. A. Erdely, M. Dahm, B. T. Chen, P. C. Zeidler-Erdely, J. E. Fernback, M. E. Birch, D. E. Evans, M. L. Kashon, J. A Deddens, T. Hulderman, S. A. Bilgesu, L. Battelli, D. Schwegler-Berry, H. D. Leonard, W. McKinney, D. G. Frazer, J. M. Antonini, D. W. Porter, V. Castranova, M. K. Schubauer-Berigan, Carbon nanotube dosimetry: from workplace exposure assessment to inhalation toxicology, *Part. Fibre Toxicol.* 10 (2013) 53.

13. G. Oberdörster, T. A. J. Kuhlbusch, In vivo effects: Methodologies and biokinetics of inhaled nanomaterials, *Nanoimpact* 10 (2018) 38-60.

14. A. D. Maynard, R. J. Aitken, T. Butz, V. Colvin, K. Donaldson, G. Oberdörster, M. A. Philbert, J. Ryan, A. Seaton, V. Stone, S. S. Tinkle, L. Tran, N. J. Walker, D. B. Warheit, Safe handling of nanotechnology, *Nature* 444 (2006) 267-269.

15. Occupational Safety and Health Administration (OSHA). https://www.osha.gov/Publications/OSHA_FS-3634.html (accessed 5 July 2018).

16. Centers for Disease Control and Prevention, National Institute of Occupational Safety and Health (CDC-NIOSH). (https://www.cdc.gov/niosh/docs/2018-121/pdfs/2018-121.pdf (accessed 5 July 2018).

17. Harvard University. Environmental Health and Safety. https://www.ehs.harvard.edu/sites/ehs.harvard.edu/files/lab_glove_policy_poster_detailed.pdf (accessed 5 July 2018)

18. V. Gomez, A. Clemente, S. Irusta, F. Balas, J. Santamaria, Identification of TiO_2 nanoparticles using La and Ce as labels: application to the evaluation of surface contamination during the handling of nanosized matter, *Environ. Sci. Nano* 1 (2014) 496-503.

19. V. Gomez, S. Irusta, F. Balas, N. Navascues, J. Santamaria, Unintended emission of nanoparticle aerosols during common laboratory handling operations, *J. Hazard. Mater.* 279 (2014) 75-84.

20. M. Hedmer, L. Ludvigsson, C. Isaxon, P. T. Nilsson, V. Skaug, M. Bohgard, J. H. Pagels, M. E. Messing, H. Tinnerberg, Detection of multi-walled carbon nanotubes and carbon nanodiscs on workplace surfaces at a small-scale producer, *Ann. Occup. Hyg.* 7 (2015) 836-852.

ACCEPTED MANUSCRIPT

21. Y. Ding, T. A. J. Kuhlbusch, M. Van Tongeren, A. Sanchez, I. Tuinman, R. Chen, I. Larraza, U. Mikolajczyk, C. Nickel, J. Meyer, H. Kaminski, W. Wohlleben, B. Stahlmecke, S. Clavaguera, M. Riediker, Airborne engineered nanomaterials in the workplace—a review of release and worker exposure during nanomaterial production and handling processes, *J. Hazard. Mater.* 322 (2017) 17-28.

22. C. S. J. Tsai, Contamination and release of nanomaterials associated with the use of personal protective clothing, *Ann. Occup. Hyg.* 59 (2015) 491-503.

23. T. Schneider, K. A. Jensen, Relevance of aerosol dynamics and dustiness for personal exposure to manufactured nanoparticles, *J. Nanopart. Res.* 11 (2009) 1637-1650.

24. R. A. Murray, A. Escobar, N. G. Bastus, P. Andreozzi, V. Puntes, S. E. Moya, Fluorescently labelled nanomaterials in nanosafety research: Practical advice to avoid artefacts and trace unbound dye, *Nanoimpact* 9 (2017) 102-113.

25. A. Clemente, F. Balas, M. P. Lobera, J. Santamaria, Versatile hollow fluorescent metal-silica nanohybrids through a modified microemulsion synthesis route, *J. Coll. Int. Sci.* 513 (2018) 497-504.

26. D. Zhang, Z. Wu, J. Xu, J. Liang, J. Li, W. Yang, Tuning the emission properties of $Ru(phen)_3^{2+}$ doped silica nanoparticles by changing the addition time of the dye during the Stöber process, *Langmuir* 26 (2010) 6657-6662.

27. A. Clemente, F. Balas, M. P. Lobera, S. Irusta, J. Santamaria, Fluidized bed generation of stable silica nanoparticle aerosols, *Aerosol Sci. Technol.* 47 (2013) 867-874.

28. A. Clemente, F. Balas, M. P. Lobera, J. Santamaria, A versatile generator of nanoparticle aerosols. A novel tool in environmental and occupational exposure assessment, *Sci. Total Environ.* 625 (2018) 978-986.

29. W. C. Hinds, Aerosol Technology: Properties, Behavior, and Measurement of Airborne Particles, Second ed., Wiley-Interscience, New York, 1999.

ACCEPTED MANUSCRIPT

30. J. H. Vincent, Aerosol Sampling: Science, Standards, Instrumentation and Applications, Wiley-Interscience, New York, 2007.

31. A. Clemente, N. Moreno, M. P. Lobera, F. Balas, J. Santamaria, Fluorescently-labeled SiO_2 nanoparticles as tracers in natural waters: dependence of detection limits on environmental conditions, *Environ. Sci. Nano* 3 (2016) 631-637.

32. S. Rengasamy, R. Shaffer, B. Williams, S. Smit, A comparison of facemask and respirator filtration test methods, *J. Occup. Environ. Hyg*. 14 (2017) 92-103.

33. C. Paulausky, Clearing the air about disposable dust masks, *Occup. Health & Safety* (2015). https://ohsonline.com/Articles/2015/11/01/Clearing-the-Air-About-Disposable-Dust-Masks.aspx (accessed 5 July 2018).

Figure captions

Figure 1. The TEM and SEM images showed that fluorescent labeling led to spherical nanoparticles with size distributions centered about 80 nm for $Ru(phen)_3@SiO_2$ (a) and about 60 nm for $FITC@SiO_2$ (d) with a very monodisperse size distributions (b, e). Laser irradiation at 405 nm in water suspensions (10 μg/ml) induced the fluorescent emission (c, f) of labeled nanoparticles in the characteristic red and green colors.

Figure 2. Aerosol generators deliver a steady air stream with particle concentration over 10^5 particles/cm^3 for periods up to several hours with count median diameters (CMD) of *ca.* 90 nm for $Ru(phen)_3@SiO_2$ (a) and 70 nm for $FITC@SiO_2$ (b), similar to the primary particle sizes obtained by TEM. The SEM images of $Ru(phen)_3@SiO_2$ (c) and $FITC@SiO_2$ (d) nanoparticles captured in gas phase confirmed the generation of primary particle aerosols.

ACCEPTED MANUSCRIPT

Figure 3. Deposition of nanoparticles in a simulated accidental aerosol generation during transfer of nanoparticles: aggregates of microns and even tens of microns size are formed during transfer of nanoparticles between two beakers and collected in a carbon tape located in the work area (a-c). The fluorescent emission of $Ru(phen)_3@SiO_2$ nanoparticles under LED illumination at 405 nm was apparent in several areas (walls, handling area, floor, gloves), inside the testing glove box (d, e). Nanoparticle contamination is not perceptible under daylight (f), but is easy to spot under laser irradiation at both daylight (g) and in dark (h). NOTE: images (d), (e) and (h) were taken through an violet light block filter.

Figure 4. Visible light image of the convoluted glass pipe system used in the nanoparticle aerosol experiments (a). Same system viewed under 365-nm light after flowing $FITC@SiO_2$ nanoparticle aerosol (b), where particle deposition is clearly visible (most highly loaded areas marked with a circle). Details of contamination at preferential locations revealed by illumination with 365-nm or 405-nm light after passing $Ru(phen)_3@SiO_2$ or $FITC@SiO_2$ nanoparticle aerosols (c-g).

Figure 5. Top, from left to right: Scheme of the different layers in the mask filter. Layers 1 and 2 are thin and are composed by large fibers, while layer 3 is thick and consists of thin, entangled fibers. Next two pictures are compositions showing natural light images (right side) and pictures taken under 405 or 365 nm LED light. Bottom, from left to right: First four pictures show the confocal microscopy images of the upstream surfaces of layers 1, 2 and 3, and of the downstream surface of layer 3 for masks exposed to $Ru(phen)_3@SiO_2$ (orange) or $FITC@SiO_2$ (green) nanoparticles, respectively. The last two panels display the optical density confocal microscopy images taken from the upstream side of layers 1, 2 and 3, and from the downstream side of layer 3 (NOTE: layers are not to scale, in layer 3 assessment is limited to the depth of penetration of the confocal microscope under the conditions used, approximately 90 μm).

Figure 6. Visual estimation of the limit of detection (LoD) when fluorescent nanoparticles were diluted with non-fluorescent matter. A 200-μl drop of an ethanolic suspension of $Ru(phen)_3@SiO_2$

ACCEPTED MANUSCRIPT

nanoparticles diluted with the desired amount of non-labeled silica is allowed to evaporate on a 1-cm circular glass slide for several minutes. The fluorescence emission was observed under a 1-mW 405 nm laser light and the image was taken through a violet color-blocking filter.

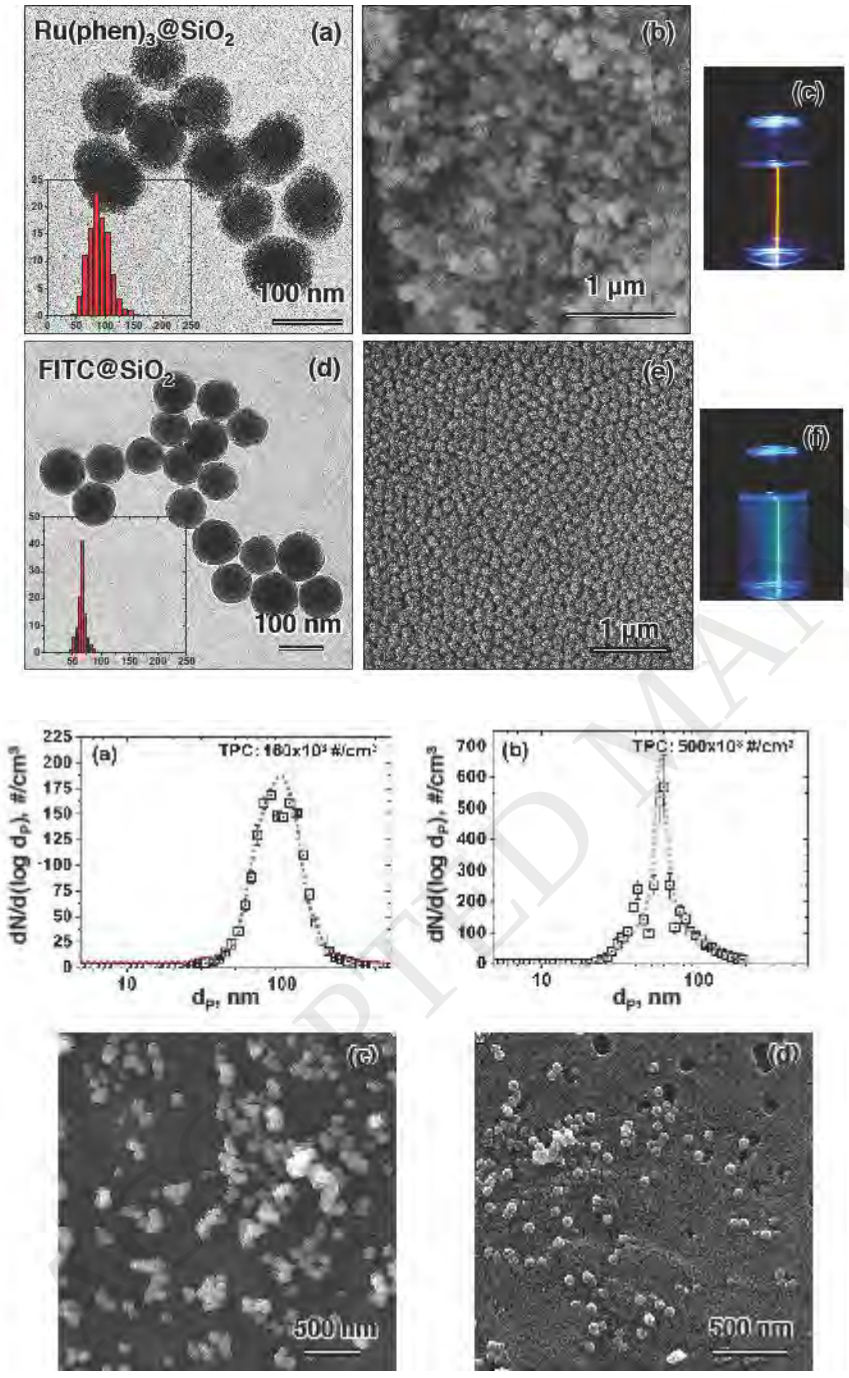

ACCEPTED MANUSCRIPT

ACCEPTED MANUSCRIPT

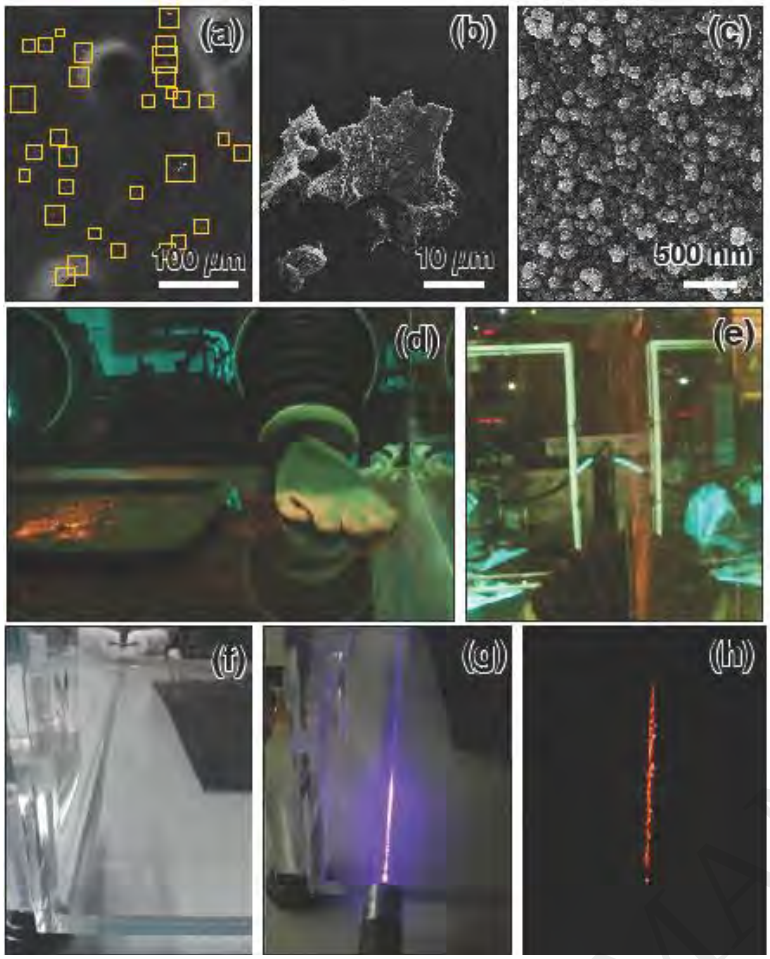

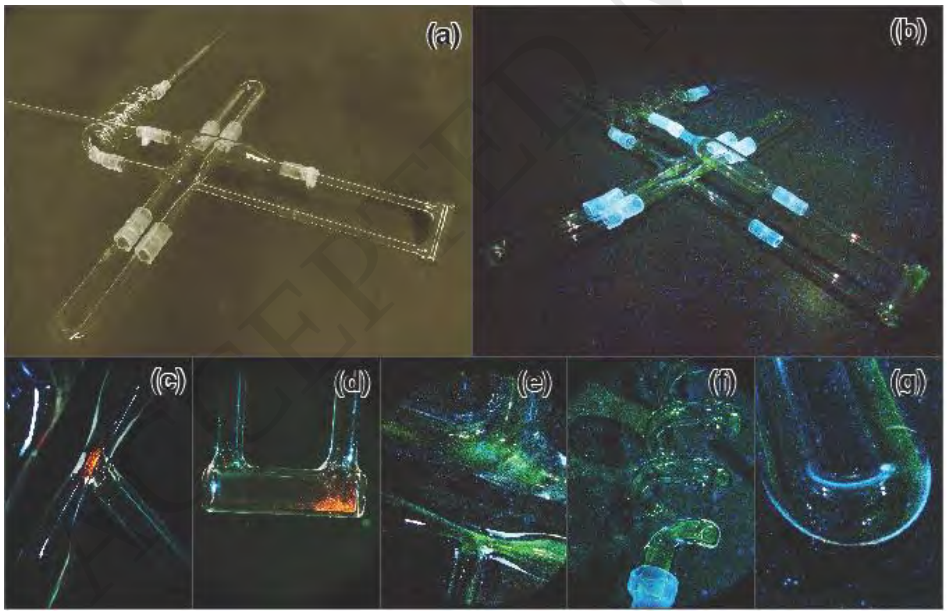

ACCEPTED MANUSCRIPT

ACCEPTED MANUSCRIPT

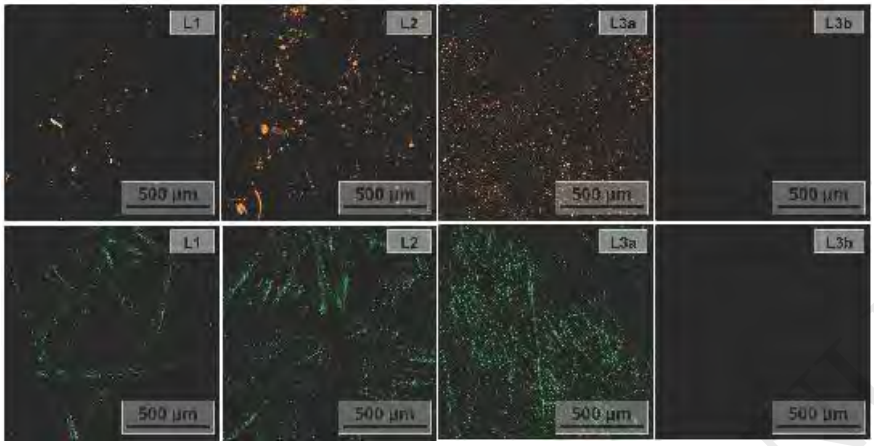

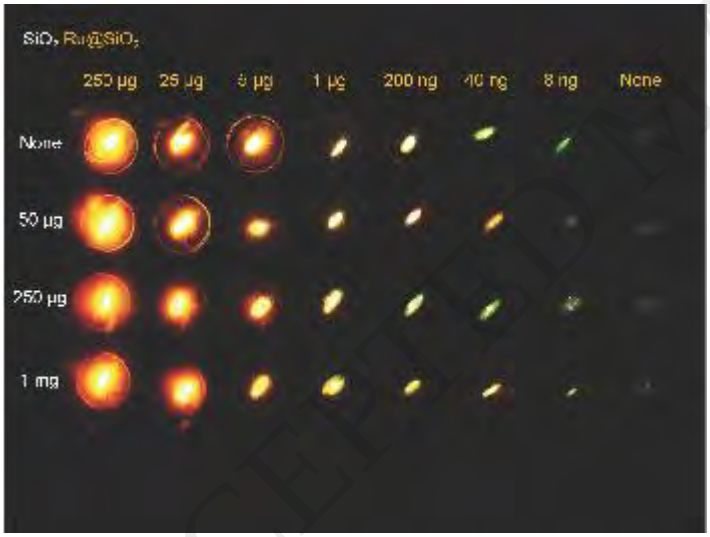

ACCEPTED MANUSCRIPT